MORPHOLOGY, OPTICAL AND LUMINESCENCE PROPERTIES OF ZnO LAYERS DOPED WITH Al OR Ag AND CO-DOPED WITH RARE EARTH IONS

A. V. ROGACHEV[1], A. V. SEMCHEMKO[1], V. E. GAISHUN[1], E. V. RUSU[2], V. V. URSAKI[2], N. CURMEI[2], V. ZALAMAI[3]

[1]Francisk Skorina Gomel State University, Gomel, 246019, Republic of Belarus
[2]Institute of Electronic Engineering and Nanotechnology of the Academy of Sciences of Moldova, Academy str. 3/3, MD-2028 Chisinau, Moldova, E-mail: ursaki@yahoo.com
[3]Institute of Applied Physics, Academy of Science of Moldova, Chisinau, MD-2028, Republic of Moldova

Received February 16, 2017

Abstract. In this paper we propose a method for measuring the negative refraction index of films of optically transparent materials. Morphological, optical and luminescence properties of rare earth doped ZnO layers prepared by a sol-gel method with spin-coating, by magnetron sputtering, and by aerosol spray pyrolysis are investigated in this paper by means of atomic force microscopy (AFM), optical absorption and luminescence spectroscopy at room temperature. It was found that the morphology of layers prepared by spin-coating is influenced by rare earth doping, a mechanism being proposed for the explanation of this influence. Optical transmission up to 90%, and the absorption edge in the region of exciton resonances have been demonstrated in ZnO layers prepared by sol-gel spin coating. The photoluminescence characterization of ZnO layers doped with Eu3+ and Er3+ ions suggests that the rare earth ion is incorporated into the wurtzite ZnO host by substitution on the Zn sublattice.

Key words: Zinc oxide, thin layer, sol-gel, spin coating, magnetron sputtering, rare earth, photoluminescence.

1. INTRODUCTION

Zinc oxide is a semiconductor widely used in various optoelectronic application, particularly in solar cells based on Si or $Cu(In,Ga)Se_2$ (CIGS) thin films with ZnO:Al transparent window layer, due to the wide band gap, high transparency, and low resistivity, [1–6]. Carrier transport has been analyzed in ZnO/SiO_2/n-Si solar cell as a function of the barrier (SiO_2) layer thickness and the electron concentration in the ZnO layer. The optimum thickness of the barrier layer of around 2 nm was found, and it was shown that decrease of ZnO layer optical transmittance due to the increase of carrier concentration does not impact the cell performance.

On the other hand, the decrease of work function of ZnO with increasing the carrier concentration leads to increase of cell efficiency [1]. ZnO nanostructured layers (*i.e*. ZnO nanowhisker arrays, or ZnO films deposited on a porous silicon layer) are also used for increasing the silicon solar cells efficiency, due to the efficient antireflection coating provided by nanostructured ZnO film [2, 3]. Planar and textured single-crystalline Si solar cells have been fabricated on industrial scale using ZnO nanorods antireflection coating [4].

Record efficiencies exceeding 20 % have been reported for CIGS solar cells with aluminum doped ZnO layers [5, 6]. Sputtering made ZnO thin films have been also used as an electron-transport layer in a regular planar perovskite solar cell [7]. Therefore, production of ZnO films compatible with Si-based and other technologies is important for industrial applications.

A single-junction solar cell absorbs light in a quite narrow spectral range, since it is transparent to photons with energies below the bandgap energy, from the one side, and the higher-energy part of the sunlight spectrum is lost due to the thermalization of high-energy (UV) photons, on the other side. One way of increasing the efficiency of solar cells, including those with ZnO layers is broadening the absorption range of the cell. Such broadening can be performed by up-conversion and down-conversion techniques, which convert the incident solar light into a spectrum that matches the absorption of the active layer in solar cells. The progress achieved on various types of efficient upconversion materials and their use in a series of solar cells, including silicon solar cells (crystalline and amorphous), gallium arsenide (GaAs) solar cells, dye-sensitized solar cells, and other types of solar cells was summarized in a recent paper [8]. Utilizing of concentrating integrated optics, *i.e.* tapered and parabolic concentrators, have been recently proposed to enhance up conversion in photovoltaics [9]. In such a case, the sub-band-gap photons are independently concentrated on the up-conversion layer.

One route for widening absorption range is the conversion luminescence by doping rare-earth compounds. In some cases, doping with 3^+ rare-earth ions performs two functions: increases incident light harvest by spectral conversion, which results in increasing photocurrent of the cell, and changes the Fermi level in the active layer and thus heightens photovoltage, as demonstrated in dye-sensitized solar cells based on TiO_2 films doped with YF_3:Eu^{3+} [10], or in organic/inorganic hybrid solar cells doped with Y_2O_3: Dy^{3+} [11]. Up-conversion by lanthanide compounds has been discussed in various host materials, including those used in thin-film silicon solar cell [12].

Blue, green, and red up-conversion was realized in some ZnO structures such as Er^{3+}-doped ZnO nanospheres and nanocrystals [13, 14], ZnO:Er and ZnO:Er:Yb thin films [15, 16], upon excitation with infrared 980 nm radiation. A down conversion ZnO:Eu^{3+},Dy^{3+} material synthesized by precipitation method was used

as photo-anode of dye-sensitized solar cells [17]. This material converts blue to red light emission, corresponding to the absorption region of the dye N719.

However, the data about the incorporation of rare earth ions into the ZnO wurtzite lattice are scarce in the literature. The goal of this paper is to investigate the influence of rare earth doping on the morphology and optical properties of ZnO layer prepared by different methods and to demonstrate the incorporation of Er^{3+} and Eu^{3+} ions into the crystal lattice of ZnO films prepared by a sol-gel method with spin-coating.

2. SAMPLE PREPARATION

ZnO layers doped with Al or Ag and co-doped with rare earth elements such as Eu, Er, or Tb and Yb have been prepared by a sol-gel method with spin-coating. Zinc acetate dihydrate ($Zn(CH_3COO)_2{\cdot}2H_2O$) was used as Zn source, and dimethylforamide (C_3H_7NO), 2-methoxyethanol ($C_3H_8O_2$), or isopropyl alcohol were used as solvent, while ethanolamine served as stabilizing component. Doping with Al and Eu, for instance, was performed by adding $Al(NO_3)_3$ and $EuCl_3$, or $Eu(TTA)_3(Ph_3PO)_2$ to the solution subjected to ultrasonic stirring when preparing the sol. The prepared sol was spin-coated on silica glass or Si(100) substrates. The samples were heat-treated at the temperature of 150^{o}C during 10 minutes after each spin-coating process. The process was repeated until a needed layer thickness was produced. After that, the sample was subjected to thermal treatment at 500^{o}C during 45 minutes.

ZnO layers co-doped with Al and Sm have been also produced by magnetron sputtering from a Zn+5%Al+2%Sm target followed by thermal treatment in air at 500^{o}C during 45 minutes.

Some samples have been prepared by aerosol spray pyrolysis with a special injector under the pressure of an oxygen flow. The chemical solution spray rate was controlled by means of a system with stepper motor controlled by a computer, so that the volume of 2–5 mL of the chemical solution is deposited on the substrate during 8–15 min. Zinc acetate dihydrate ($Zn(CH_3COO)_2{\cdot}2H_2O$ with concentration of 0.05–0.1 M dissolved in a dimethylforamide (C_3H_7NO) or 2-methoxyethanol ($C_3H_8O_2$) solvent with monoethanolamin (C_2H_7NO) as stabilizer were used as spray chemical solution.

3. MORPHOLOGY CHARACTERIZATION

The AFM investigations of the produced ZnO layers co-doped with Al and rare earth elements (Eu or Er) shown that they consist of a texture combining smaller crystallites of submicron sizes and larger crystallites of the order of 1 μm, the height of these crystallites being larger for samples co-doped with Er (Fig. 1).

So, that the roughness of layers is 100–200 nm and 50–150 nm for samples co-doped with Er and Eu, respectively.

The samples co-doped with Ag and rare earth elements exhibit a more uniform crystallite size distribution, all the crystallites being of submicron sizes. In contrast to samples doped with Al, in samples doped with Ag the roughness is larger for samples co-doped with Eu as compared to those co-doped with Er, since some crystallites are higher in samples co-doped with Eu (Fig. 1).

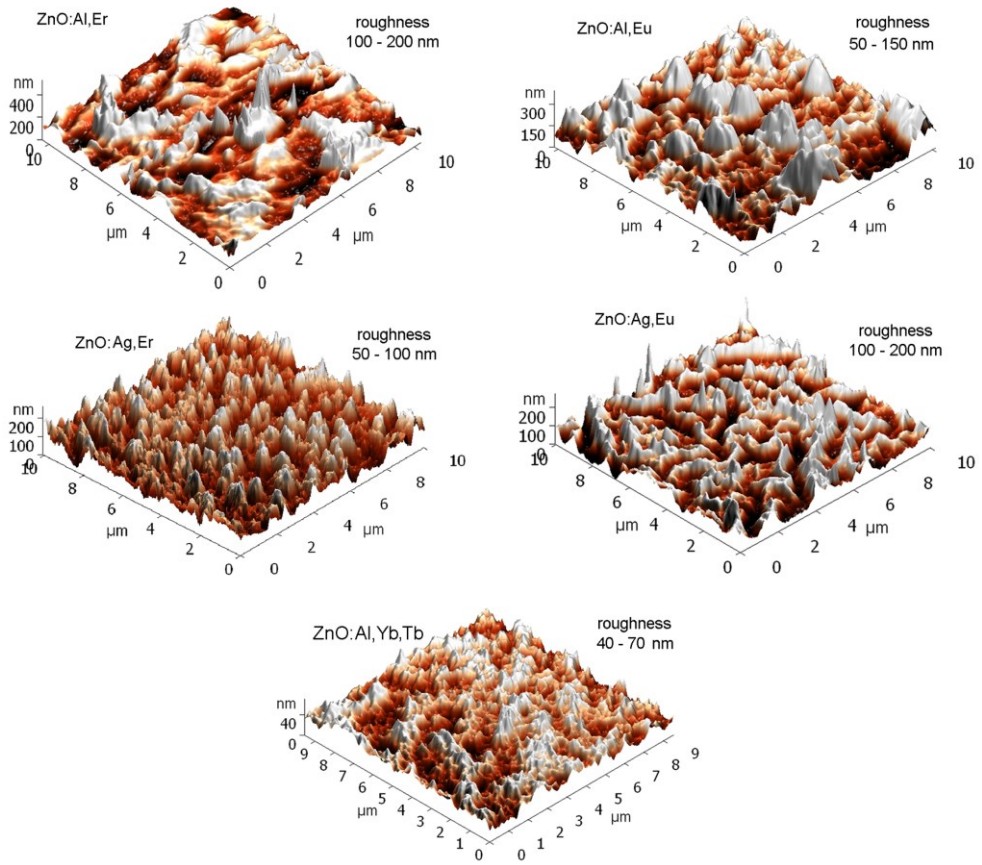

Fig. 1 – 3D AFM images of sol-gel prepared ZnO layers doped with Al or Ag and co-doped with rare earth elements.

The produced morphologies are explained by competing processes occurring during sol-gel deposition of ZnO layers containing heavy elements (Er, Eu, Yt, Tb): migration of atoms on the substrate surface, and crystallization of sol agglomerates at nucleation centers. The presence of heavy elements in the sol leads

to decreasing the velocity of atoms surface migration. As a result, the coalescence of islands and the formation of a continuous mono-layer on the substrate occur significantly slower than the crystallization at nucleation centers. Layers with a high degree of roughness are produced as a result of dominating crystal growth on the islet fragments, while the layer roughness depends on the type of the doping impurity. Layers with lowest roughness (40–70 nm) are produced upon co-doping with Al,Yb,Tb.

More uniform ZnO layers with crystallite sizes around 200 nm have been produced by aerosol spray pyrolysis (Fig. 2a). A similar background layer with crystallite size of the order of 200 nm was realized in ZnO layers doped with Er in a magnetron sputtering process. However, some larger crystallites were formed on this background similarly to rare earth doped layers produced by sol gel spin-coating (Fig. 2b).

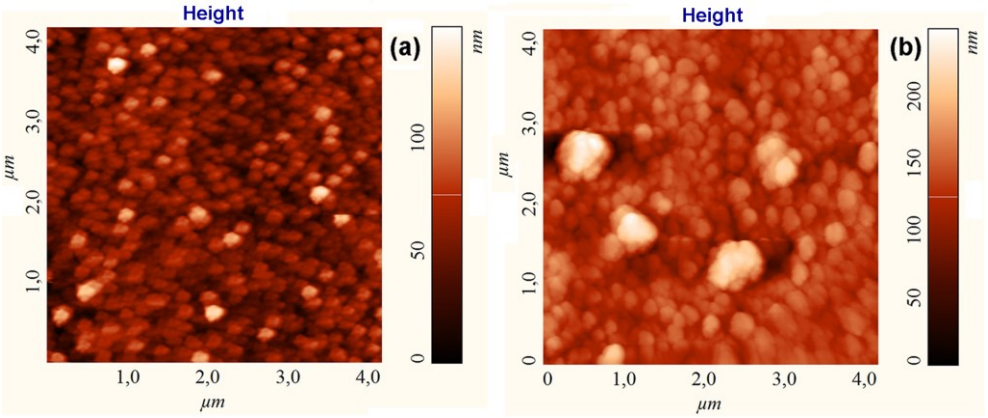

Fig. 2 – AFM images of ZnO layers prepared by aerosol spray pyrolysis (a) and Er-doped ZnO layers deposited by magnetron sputtering (b).

4. OPTICAL CHARACTERIZATION

The optical transmission of ZnO layers prepared by sol-gel spin coating is around 90% (Fig. 3a), a parameter which is important when such layers are used as transparent contacts to solar cells. The transparency of the layer produced by magnetron sputtering is less, as shown by curve 4 in Fig. 2a. The Tauc plot was plotted for estimation of the optical gap of the produced layers (Fig. 3b). The deduced optical gap value from this plot is in the range of 3.28–3.29 eV for layer prepared by sol-gel spin coating, a value which is nearly equal to the exciton resonances in ZnO at room temperature. For layers prepared by magnetron sputtering the estimated value of the optical gap is lower (about 3.24 eV), which is

an indication of a lower optical quality, suggesting the presence of an impurity band near the absorption ban edge (curve 4 in Fig. 3b).

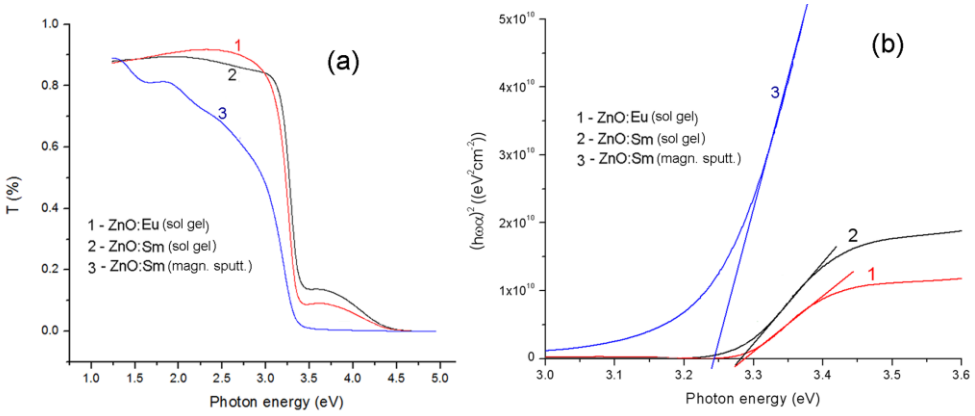

Fig. 3 – Spectra of optical transmission (a), and Tauc plot for ZnO rare earth doped ZnO layers prepared by different methods (b).

5. PHOTOLUMINESCENCE SPECTROSCOPY ANALYSIS

The activation of rare earth ions into the ZnO host was investigated by means of photoluminescence spectroscopy. A series of narrow emission bands in then range of 540–550 nm are observed in the PL spectra of ZnO layers doped with Er impurity (Fig. 4).

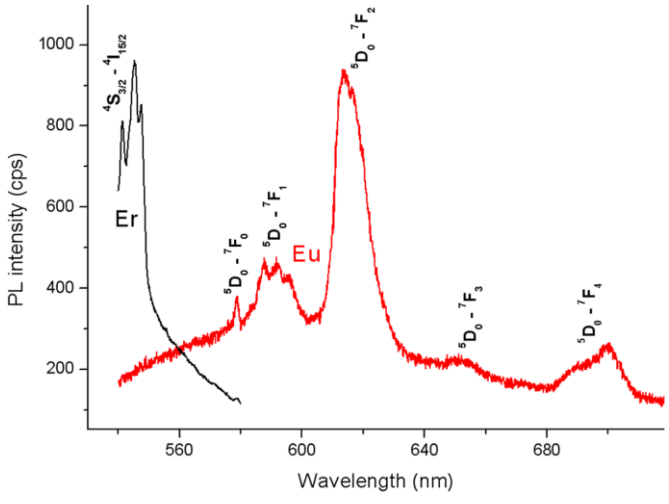

Fig. 4 – PL spectra of Er and Eu doped ZnO layers produced by spin coating.

These lines are due to transitions from the excited $^4S_{3/2}$ level to the ground $^4I_{15/2}$ level of the Er^{3+} ions. Usually, the rare earth ions are incorporated in the Zn sites with C_{3v} symmetry of the wurtzite ZnO lattice. According to group-theoretical methods [18, 19], the $^4S_{3/2}$ and $^4I_{15/2}$ energy states of Er^{3+} in C_{3v} symmetry are split into $\Gamma_4+(\Gamma_5 + \Gamma_6)$, and $5\Gamma_4+3(\Gamma_5+\Gamma_6)$, Stark levels, respectively. Therefore, eight emission lines should be observed when the electrons are transferred from the lowest level of the excited states $^4S_{3/2}$ state to the split levels of the ground $^4I_{15/2}$ state. However, only five PL bands are deduced from the deconvolution of the PL spectrum as shown in Fig. 5.

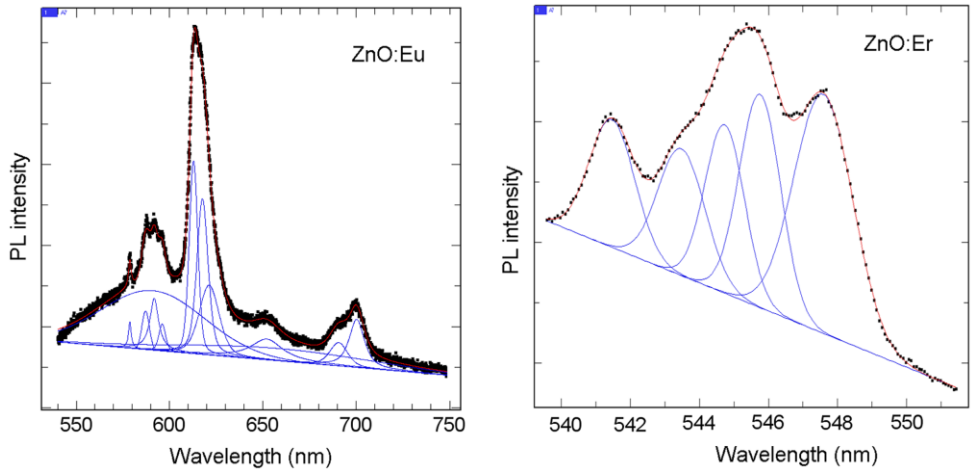

Fig. 5 – Deconvolution of the Eu and Er doped ZnO layers produced by spin coating.

This observation can be explained either by the fact that some of the Stark split manifold of $^4I_{15/2}$ levels are situated very close to each other, so that the respective transitions can not be resolved in the PL spectrum, or by the fact that the laser radiation is polarized, and in C_{3v} site symmetry, one can expect at most five emission transitions between $^4S_{3/2}$ and $^4I_{15/2}$ free ion states in π-polarization [20].

The PL spectrum of Eu-doped samples consists of a series of PL bands related to the Eu^{3+} 4f-4f intrashell transitions superimposed on two broad PL in the orange-red spectral region. The orange-red broadband emission in ZnO is commonly believed to come from structural defects, such as interstitial oxygen [21, 22]. The lines related to the Eu^{3+} 4f-4f intrashell transitions are summarized in Table 1.

Table 1

The PL bands related to the Eu^{3+} 4f-4f intrashell transitions in ZnO laters

Band label	1	2	3	4	5	6	7	8	9	10
Wavelength, nm	578	587	592	596	613	617	622	651	690	700
Transition	$^5D_0 \rightarrow {}^7F_0$	$^5D_0 \rightarrow {}^7F_1$			$^5D_0 \rightarrow {}^7F_2$			$^5D_0 \rightarrow {}^7F_3$	$^5D_0 \rightarrow {}^7F_4$	

All the observed lines are consistent with Eu^{3+}-related emission from $^5D_0 \rightarrow {}^7F_j$ (J = 1,2,3,4) transitions. As mentioned above, it is well documented that rare earth ions, including Eu^{3+} ions are usually incorporated in II-VI compounds by substitution on the metal sublattice with C_{3v} site symmetry. The C_{3v} site symmetry splits ground $^7F_{2-5}$ levels. Theoretically, the $^7F_2$ level gives three crystal field levels of A_1 and 2E with C_{3v} symmetry [23, 24], which gives rise to PL lines centered at 613, 617, and 622 nm. This $^5D_0 \rightarrow {}^7F_2$ emission comes from an allowed electric-dipole (ED) transition [24, 25, 26], which results in a large transition probability in the crystal fields without inversion symmetry. The lines at 587, 592, and 596 nm are due to $^5D_0 \rightarrow {}^7F_1$ transitions. The $^7F_2$ level should give only two crystal field levels in a site with C_{3v} symmetry [24]. The presence of three lines related to $^5D_0 \rightarrow {}^7F_1$ transitions, along with the observation of the $^5D_0 \rightarrow {}^7F_0$ transition, which may only be activated by Eu^{3+} at interstitial sites with lower symmetry than C_{3v} [27, 28], suggests that some of Eu^{3+} ions are incorporated into sites with the symmetry different from C_{3v}.

In contrast with $^5D_0 \rightarrow {}^7F_2$ transition, the $^5D_0 \rightarrow {}^7F_1$ transition is a magnetic-dipole (MD) one [24, 25, 26]. When the Eu ion is placed at a center of symmetry, ED transitions between the $4f^6$ levels are strictly forbidden by the Laporte selection rule (equal parity) while MD transitions are allowed. Thus, the intensity ratio of $^5D_0 \rightarrow {}^7F_2$ to $^5D_0 \rightarrow {}^7F_1$ transition, known as the asymmetry ratio, would be zero when Eu ion is at a center of perfect symmetry, but could be quite large for distorted sites. The asymmetry ratio in our samples is ~5. Such a high value is explained by the lack of inversion symmetry when the Eu^{3+} ion is incorporated into wurtzite ZnO host by substitution on the Zn sublattice. This lack of inversion symmetry produces strong ligand crystal fields and thereby relaxes the Laporte selection rule.

6. CONCLUSIONS

The results of this study demonstrate that the morphology of ZnO layers doped with Al or Ag is impacted by co-doping with rare earth elements in a sol-gel method with spin-coating. The impact is explained by competing processes occurring during sol-gel deposition such as migration of atoms on the substrate surface and crystallization of sol agglomerates at nucleation centers. The presence of heavy elements in the sol impedes the atom migration, favoring the crystal growth on islet fragments, and deposition of layers with larger roughness. The deposition process is also influenced by the interaction of doping (Al or Ag) and co-doping (Eu, Er, Yb, or Tb) impurities. As a result, in samples doped with Al the roughness is larger for samples co-doped with Eu as compared to those co-doped with Er, while the situation is *vice-versa* in samples doped with Ag. Layers with lowest roughness are produced upon co-doping with Al,Yb,Tb. The optical properties are less impacted by rare earth doping, but more dependent on the deposition technology. Layers with optical transmission up to 90%, and the absorption edge in the region of exciton resonances are prepared by sol-gel spin coating. The analysis of photoluminescence spectra suggests that the Eu^{3+} and Er^{3+} ions are incorporated into the wurtzite ZnO host by substitution on the Zn sublattice.

Acknowledgments. This work was supported by the Academy of Sciences of Moldova under the Grants Nos 15.817.02.08A and 15.820.18.02.05BGA.

REFERENCES

1. W. W. Wenas, S. Riyadi, Sol. Energ. Mat. Sol. C. **90**, 3261–3267 (2006).
2. X. Yu, D. Wang, D. Lei, G. Li, D. Yang, Nanoscale Res. Lett. **7**, 306 (2012).
3. K. A. Salman, K. Omar, Z. Hassan, Sol. Energy **86**, 541–547 (2012).
4. P. Aurang, O. Demircioglu, F. Es, R. Turan, Hu. E. Unalan, J. Am. Chem. Soc. **96**, 1253–1257 (2013).
5. A. Chirila, P. Reinhard, F. Pianezzi, P. Bloesch, A. R. Uhl, C. Fella, L. Kranz, D. Keller, C. Gretener, H. Hagendorfer, D. Jaeger, R. Erni, S. Nishiwaki, S. Buecheler, A. N. Tiwari, Nat. Mater. **12**, 1107–1111 (2013).
6. P. Jackson, D. Hariskos, E. Lotter, S. Paetel, R. Wuerz, R. Menner, W. Wischmann, M. Powalla, Prog. Photovoltaics **19**, 894–897 (2011).
7. Z.-L. Tseng, C.-H. Chiang, C.-G. Wu, Sci. Rep. **5**, 13211 (2015).
8. Y. Shang, S. Hao, C. Yang, G. Chen, Nanomaterials **5**, 1782–1809 (2015).
9. G. E. Arnaoutakis, J. Marques-Hueso, A. Ivaturi, K. W. Kramer, S. Fischer, J. C. Goldschmidt, B. S. Richards, Opt. Express **22**, A452-A464 (2014).
10. J. Wu, J. Wang, J.G. Lin, Y. Xiao, G. Yue, M. Huang, Z. Lan,Y. Huang, L. Fan, S. Yin, T. Sato, Sci. Rep. **3**, 2058 (2013).
11. Z. Chen, Q. Li, C. Chen, J. Du, J. Tong, X. Jin, Y. Li, Y. Yuan, Y. Qin, T. Wei, W. Sun, Phys. Chem. Chem. Phys. **16**, 24499–24508 (2014).
12. W.G. van Sark, J. de Wild, J.K. Rath, A. Meijerink, R.E. Schropp, Upconversion in solar cells, Nanoscale Res. Lett. **8**, 81–85 (2013).

13. J. Geng, G.-H. Song, J.-J. Zhu, J. Nanomater. **2012**, 317857 (2012).
14. X. Wang, X. Kong, Y. Yu, Y. Sun, H. Zhang, J. Phys. Chem. C **111**, 15119–15124 (2007).
15. M. Llusca, J. Lopez-Vidrier, A. Antony, S. Hernandez, B. Garrido, J. Bertomeu, Thin Solid Films **562**, 456–461 (2014).
16. R. Elleuch, R. Salhi, J.-L. Deschanvres, R. Maalej, RSC Adv. **2015**, 60246–60253 (2015).
17. N. Yao, J. Huang, K. Fu, S. Liu, D. E, Y. Wang, X. Xu, M. Zhu, B. Cao, J. Power Sources **267**, 405–410 (2014).
18. G. F. Koster, J. O. Dimmock, R. G. Wheeler, H. Statz, *Properties of 32 Point Groups,* MIT, Cambridge, MA, 1963.
19. M.-S. Jin, C.-I. Lee, N.-O. Kim, W.-T. Kim, J. Korean Phys. Soc. **40**, 497–500 (2002).
20. S.-H. Choe, H.-L. Park, W.-T. Kim, J. Korean Phys. Soc. **38**, 155–157 (2001).
21. Y.W. Heo, D.P. Norton, S.J. Pearton, J. Appl. Phys. **98**, 073502 (2005).
22. Y. B. Zhang, G. K. L. Goh, K. F. Ooi, S. Tripathy, J. Appl. Phys. **108**, 083716 (2010).
23. S. Fujihara, A. Suzuki, T. Kimura, J. Appl. Phys. **94**, 2411–2416 (2003).
24. J. B. Gruber, U. Vetter, T. Taniguchi, G. W. Burdick, H. Hofsass, S. Chandra, D. K. Sardar, J. Appl. Phys. **110**, 023104 (2011).
25. R. D. Peacock, *in Structure and Bonding*, Ed. J.D. Dunitz, P. Hemmerich, R.H. Holm, J.A. Ibers, C.K. Jorgensen, J.B. Neilands, D. Reinen, R.J.P. Williams, Springer, Berlin, 1975, Vol. 22.
26. J. H. Kim, P. H. Holloway, J. Appl. Phys. **95**, 4787–4790 (2004).
27. T. Monteiro, C. Boemare, M.J. Soares, R.A. Sa Ferreira, L.D. Carlos, K. Lorenz, R. Vianden, E. Alves, Physica B **308–310**, 22–25 (2001).
28. C.-W. Lee, H.O. Everitt, D.S. Lee, A.J. Steckl, J.M. Zavada, J. Appl. Phys. **95**, 7717–7724 (2004).